Impulsive signaling model of cytoneme-based morphogen gradient formation

Hyunjoong Kim and Paul C Bressloff

Department of Mathematics, University of Utah 155 South 1400 East, Salt Lake City, UT 84112

E-mail: hkim@math.utah.edu; bressloff@math.utah.edu

Abstract. Morphogen protein gradients play a vital role in regulating spatial pattern formation during development. The most commonly accepted mechanism of protein gradient formation involves the diffusion and degradation of morphogens from a localized source. However, there is growing experimental evidence for a direct cell-to-cell signaling mechanism via thin actin-rich cellular extensions known as cytonemes. Recent modeling studies of cytoneme-based morphogenesis in invertebrates ignore the discrete nature of vesicular transport along cytonemes, focusing on deterministic continuum models. In this paper, we develop an impulsive signaling model of morphogen gradient formation in invertebrates, which takes into account the discrete and stochastic nature of vesicular transport along cytonemes. We begin by solving a first passage time problem with sticky boundaries to determine the expected time to deliver a vesicle to a target cell, assuming that there is a "nucleation" time for injecting the vesicle into the cytoneme. We then use queuing theory to analyze the impulsive model of morphogen gradient formation in the case of multiple cytonemes and multiple targets. In particular, we determine the steady-state mean and variance of the morphogen distribution across a one-dimensional array of target cells. The mean distribution recovers the spatially decaying morphogen gradient of previous deterministic models. However, the burst-like nature of morphogen transport can lead to Fano factors greater than unity across the array of cells, resulting in significant fluctuations at more distant target sites.

1. Introduction

Morphogen protein gradients play a vital role in regulating spatial pattern formation during development. The classical mechanism for gradient formation involves the diffusion of morphogen from a localized source combined with degradation [22, 1]. However, there is growing experimental evidence for a direct cell-to-cell signaling mechanism in invertebrates such as *Drosophila*, involving the active transport of morphogen along cytonemes, which are thin and actin-rich cellular extensions with a diameter of around 100 nm and lengths that vary from 1 to 100 μm [16, 8, 11, 12]. A number of recent modeling studies have investigated this form of cytoneme-based morphogenesis [21, 4, 10], focusing on the existence and stability of steady-state solutions, the nature of contacts between cytoneme tips and target cells, the accumulation time for establishing a morphogen gradient, and the robustness of the gradient with respect to perturbations of the morphogen production rate in the source cells. One major simplifying assumption of these models is that the number of vesicles is sufficiently large so that morphogens can be treated as a continuum "fluid" transported along a cytoneme and delivered to target cells, see Fig. 1(a). However, experimental evidence shows that morphogen vesicles are distributed as "puncta" along a cytoneme in invertebrates [9], see Fig. 1(b). This discrete feature introduces randomness in the number of morphogens within cells, but very little has been studied about the resulting stochastic nature of cytoneme-mediated cell-to-cell signaling, and its effects on robustness.

We have recently modeled the discrete and stochastic nature of cytoneme-based morphogenesis in the case of a different transport mechanism that has been observed in some vertebrates. Imaging studies in Wnt transport in zebrafish [18] and Shh transport in chicken [17] indicate that cytonemes loaded with morphogen at their tips actively and rapidly expand and contract. Once a cytoneme tip contacts a target cell, morphogen is immediately delivered to the cell in the form of a morphogen "burst". We analyzed the stochastic and burst-like nature of this form of morphogenesis using a "search-and-capture model" [5], analogous to microtubule-based models of

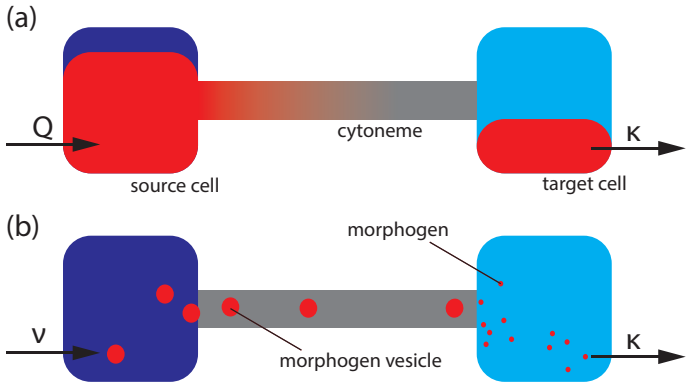

Figure 1: Models of cytoneme-mediated morphogen gradient formation in invertebrates. (a) "Fluid" model of morphogen transport in [4, 10]. This assumed that there are infinitely many vesicles. (b) Impulsive signaling model via vesicles containing finite morphogens.

the prometaphase during cell mitosis [7, 14]. The model consisted of nucleating cytonemes from a source cell that dynamically grow and shrink along the surface of a one-dimensional array of target cells until making contact with one of the target cells and delivering a morphogen burst. We showed how multiple rounds of search-and-capture, morphogen delivery, cytoneme retraction, and nucleation events leads to the formation of a morphogen gradient. We proceeded by formulating the morphogen bursting model as a queuing process, analogous to the study of protein bursting in gene networks. In order to analyze the expected times for cytoneme contact, we introduced an efficient method for solving first-passage-time problems in the presence of sticky boundaries, which exploited some classical concepts from probability theory, namely, stopping times and the strong Markov property.

In this paper we extend the mathematical framework introduced in [5] in order to develop an impulsive signaling model of morphogen gradient formation in invertebrates, which takes into account the discrete and stochastic nature of vesicular transport along cytonemes. First, in section 2 we reformulate our previous bidirectional transport model [4, 10] as a stochastic model for the transport of a single vesicle. Analogous to the nucleation of a new cytoneme in [5], we assume that if the vesicle returns to the source cell, then there is some waiting time before it is reinjected into the cytoneme. In section 3 we solve the first passage time (FPT) problem for a vesicle to be absorbed by a target cell, taking into account the sticky boundary condition at the source cell using the strong Markov property. In section 4 we use queuing theory to analyze the impulsive model of morphogen gradient formation in the case of multiple vesicles. However, it is necessary to modify the analysis of [5], since the order in which vesicles are absorbed by target cells is not necessarily the same as the order in which they are first produced (nucleated) in the source cell. We calculate the steady-state mean and variance of the morphogen distribution across a one-dimensional array of target cells. Although the mean distribution recovers the spatially decaying morphogen gradients of previous deterministic models, we show that the burst-like nature of morphogen transport can lead to Fano factors greater than unity that persist across the array of cells, resulting in significant fluctuations at more distant target sites. Finally in section 5 we introduce a differential version of the queuing model and compare its behavior with our previous "fluid" models [4, 10] using asymptotic analysis.

2. Impulsive signal transport by a single vesicle

Consider a single cytoneme of length L linking a source cell to a single target cell, see Fig. 2. Along the cytoneme, a vesicle containing morphogen is transported by a motor-cargo complex that actively moves forward and backward until it reaches the target cell. If the motor-cargo returns to the source cell, then there is some waiting time (nucleation time) before it is again injected into the cytoneme. Once the vesicle reaches the target cell, morphogen is released and generates an impulsive signal.

Let $X(t) \in [0, L]$ be the position of the vesicle at time t. Take $N(t)$ to be the current bidirectional velocity state with

$$N(t) = \begin{cases} + & \text{if } v(t) = v_+ \\ - & \text{if } v(t) = -v_- \end{cases},$$

where $v_\pm$ are the positive speed for each direction. Transitions between the two

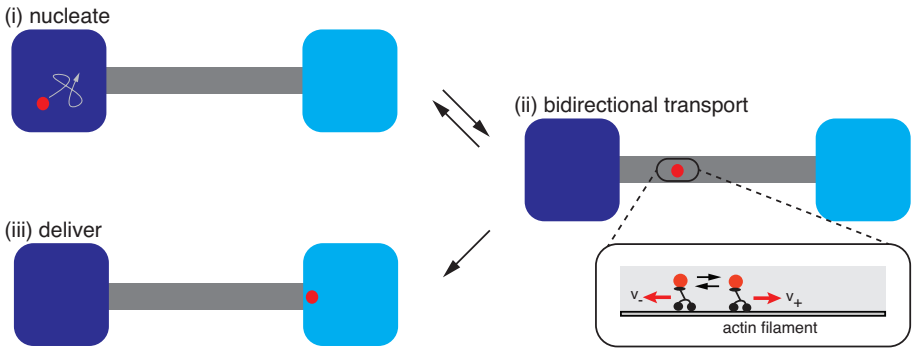

Figure 2: Stages of a single morphogen vesicle transport process generating a morphogen burst in a target cell. (i) "Nucleation" associated with production of a new vesicle or reinjection of a returning vesicle. (ii) Bidirectional transport along the cytoneme. (iii) Vesicle capture by the target cell, resulting in an impulsive morphogen signal.

velocity states occur via a two-state Markov chain:

$$\{-\} \underset{\alpha_-}{\overset{\alpha_+}{\rightleftharpoons}} \{+\}.$$

Let $p_n(x,t)$ be the probability density that at time t we have $X(t) \in [x, x+dx)$ and $N(t) = n$ where

$$p_n(x,t)dx = \mathbb{P}[x \leq X(t) < x + dx, N(t) = n].$$

The corresponding differential Chapman-Kolmogorov (CK) equation takes the form

$$\frac{\partial p_+}{\partial t} = -v_+ \frac{\partial p_+}{\partial x} - \alpha_- p_+ + \alpha_+ p_-, \tag{2.1a}$$

$$\frac{\partial p_-}{\partial t} = v_- \frac{\partial p_-}{\partial x} + \alpha_- p_+ - \alpha_+ p_-. \tag{2.1b}$$

Equation (2.1a) and (2.1b) are supplemented by the boundary conditions

$$v_+ p_+(0,t) = r_0 P_0(t), \quad p_-(L,t) = 0, \tag{2.2}$$

where $P_0(t)$ is the probability of the vesicle being located at the source cell and r_0 is an injection rate into the cytoneme. We assume that the vesicle is initially positioned in the source cell so that

$$P_0(0) = 1, \quad p_\pm(x,0) = 0,$$

for all $x \in [0, L]$. The transport component of the model couples to the probability of the vesicle in the source cell and target cells according to

$$\frac{dP_0}{dt} = v_- p_-(0,t) - r_0 P_0(t), \quad \frac{dP_1}{dt} = v_+ p_+(L,t). \tag{2.3}$$

One can extend the single cytoneme model to multiple cytonemes of length L_k linking a source cell to K_T multiple target cells, $k = 1, \cdots, K_T$, which for the sake of illustration are arranged in a one-dimensional array, see Fig. 3. Let $K(t) \in \{1, \cdots, K_T\}$ be the index of the cytoneme containing the motor cargo at time t. This leads us to specify the relative probability θ_k that a morphogen is injected into

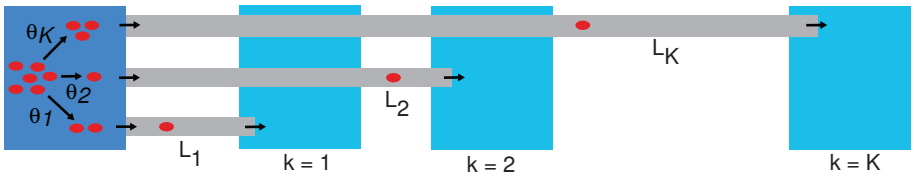

Figure 3: Schematic diagram of a one-dimensional array of target cells (labeled $k = 1, \ldots, K$), each connected to a single source cell via a cytoneme of length L_k. Vesicles in the source cell are allocated to the kth cytoneme with probability θ_k.

the kth cytoneme, where $\sum_{k=1}^{K_T} \theta_k = 1$. Let $p_n^k(x,t)$ be the probability that the vesicle is along the kth cytoneme at position x and time t. Then the evolution equation for $p_\pm^k(x,t)$ takes the same form as (2.1a) and (2.1b):

$$\frac{\partial p_+^k}{\partial t} = -v_+ \frac{\partial p_+^k}{\partial x} - \alpha_- p_+^k + \alpha_+ p_-^k, \tag{2.4a}$$

$$\frac{\partial p_-^k}{\partial t} = v_- \frac{\partial p_-^k}{\partial x} + \alpha_- p_+^k - \alpha_+ p_-^k, \tag{2.4b}$$

with corresponding boundary conditions

$$v_+ p_+^k(0,t) = r_0 \theta_k P_0(t), \quad p_-^k(L_k,t) = 0. \tag{2.5}$$

Extending (2.3) to the case of multiple target cells yields

$$\frac{dP_0}{dt} = v_- \sum_{k=1}^{K_T} p_-^k(0,t) - r_0 P_0(t), \quad \frac{dP_k}{dt} = v_+ p_+^k(L_k,t). \tag{2.6}$$

Summing (2.4a) and (2.4b) and then integrating with respect to x over the interval $[0, L_k]$ gives that

$$\frac{d}{dt} \int_0^{L_k} \left[p_+^k(x,t) + p_-^k(x,t) \right] dx = -[v_+ p_+^k(x,t) - v_- p_-^k(x,t)]|_0^{L_k}.$$

Summing with respect to k and imposing the boundary conditions (2.5) and (2.6) we have

$$\frac{dP_0(t)}{dt} + \frac{d}{dt} \sum_{k=1}^{K_T} \left[\int_0^{L_k} \left[p_+^k(x,t) + p_-^k(x,t) \right] dx + P_k(t) \right] = 0,$$

which guarantees conservation of the total probability over all events.

$$P_0(t) + \sum_{k=1}^{K_T} \left(\int_0^{L_k} \left[p_+^k(x,t) + p_-^k(x,t) \right] dx + P_k(t) \right) = 1.$$

3. First passage time problem for a single vesicle

We would like to determine the splitting probability ρ_k that the morphogen vesicle is eventually captured by the kth target, where

$$\rho_k = \lim_{t \to \infty} P_k(t), \quad \sum_{k=1}^{K_T} \rho_k = 1, \tag{3.1}$$

together with the corresponding MFPT τ_k. One way to solve the FPT problem is to Laplace transform the differential equations [7, 4]. However, one difficulty in applying Laplace transform methods to our FPT problem is that there is a sticky boundary at $x = 0$, which takes into account the exponentially distributed waiting time for reinjection of the vesicle into the cytoneme. This means that one has to keep track of the random times that the vesicle returns to the origin, resulting in a non-trivial iterative problem [7, 14]. To avoid this issue, we choose an alternative approach that exploits the strong Markov property of the stochastic process [5]. Intuitively, the strong Markov property is similar to the Markov property except that the probability of future states depends upon a stopping time, which is a random variable determined by the history of the process from the beginning to the present [15, 5]. Note, in particular that FPTs are examples of stopping times. We proceed by decomposing the transport process into a nucleation stage and a signaling transport stage, see Fig. 4(a) and [14, 5]. We first solve the FPT problem of the transport stage with an absorbing boundary condition at $x = 0$ by using the corresponding backward Kolmogorov equation. We then split all events according to whether or not the vesicle

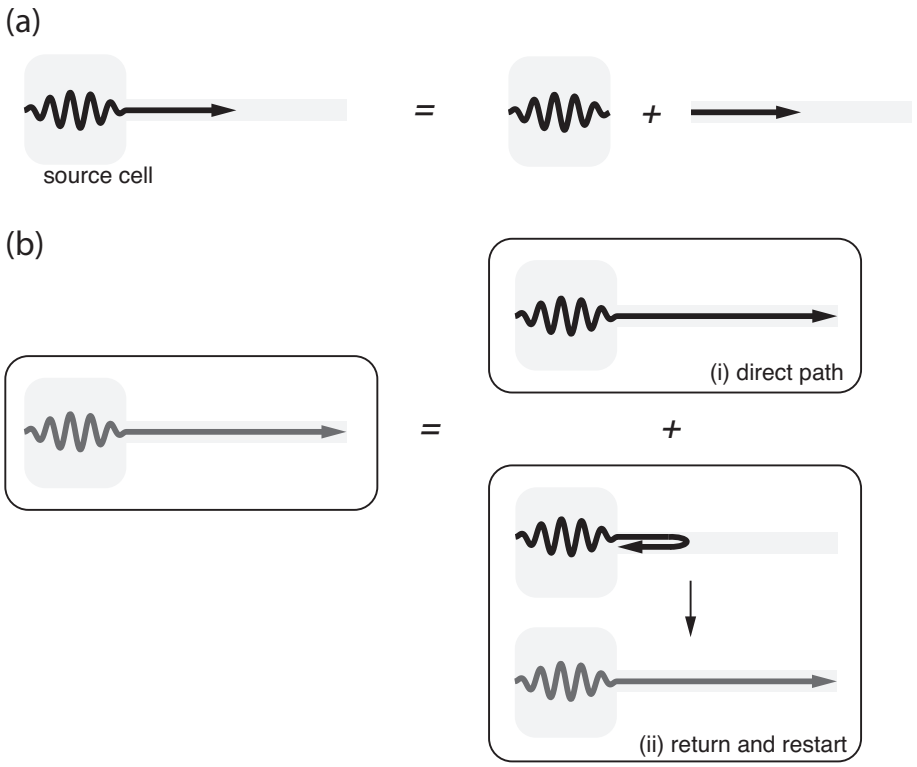

Figure 4: Decomposing MFPT problems using the strong Markov property. (a) MFPT with nucleation effect can be decomposed as the nucleation state and the transport state. (b) The unconditional MFPT (gray arrow) for a vesicle to contact the cytoneme tip starting at the source cell can be decomposed into two conditional MFPTs: (i) All paths directly reaching to the end after the nucleation (black arrow) or (ii) returning into the source cell (black arrow) and then restarting the unconditional process.

returns to the source cell, see Fig. 4(b), and use the strong Markov property to obtain the splitting probabilities and the corresponding MFPTs of the whole process.

3.1. Conditional MFPT to reach $x = L$ with an absorbing boundary at $x = 0$

We first calculate the conditional MFPT that the morphogen vesicle reaches the right-end of a single cytoneme length L before ever reaching zero, see Fig. 4(a). This means imposing absorbing boundaries at $x = 0, L$,

$$p_+(0,t) = p_-(L,t) = 0,$$

and defining the FPT

$$T_m(y) = \inf\{t \geq 0; X(t) = L, N(t) = + : X(0) = y, N(0) = m\}$$

for $0 < y < L$. Note that $T_+(L) = 0$. That is, the morphogen immediately absorbs to the target cell if it starts out anterograde state at $x = L$. The probability flux through the end $x = L$ is

$$J_m(y,t) = v_+ p_+(L,t|y,m,0).$$

It follows that for $0 < y < L$, the probability $\Pi_m(y,t)$ that the morphogen exits at $x = L$ after time t, having started in state (y,m) is

$$\Pi_m(y,t) = \int_t^\infty J_m(y,t')dt'. \tag{3.2}$$

Differentiating with respect to t gives

$$\frac{\partial \Pi_m(y,t)}{\partial t} = -J_m(y,t) = \int_0^\infty \frac{J_m(y,t')}{\partial t'}dt'.$$

Hence, using the backward CK equation leads to the pair of equations

$$\frac{\partial \Pi_+}{\partial t} = v_+ \frac{\partial \Pi_+}{\partial y} - \alpha_-[\Pi_+ - \Pi_-], \tag{3.3a}$$

$$\frac{\partial \Pi_-}{\partial t} = -v_- \frac{\partial \Pi_-}{\partial y} + \alpha_+[\Pi_+ - \Pi_-]. \tag{3.3b}$$

One can determine the boundary condition at $x = 0, L$ by noticing that if the particle starts out in the retrograde state at $x = 0$, it never reaches $x = L$, whereas if it starts out at $x = L$ in the anterograde state, it is immediately absorbed. Thus we have $\Pi_-(0,t) = 0$ and $\Pi_+(L,t) = 1$.

We can now define the splitting probability that the morphogen hits $x = L$ before $x = 0$ by introducing $\pi_m(y) = \Pi_m(y,0)$. Since

$$\left.\frac{\partial \Pi_m(y,t)}{\partial t}\right|_{t=0} = -J_m(y,0) = 0,$$

for $y \in (0,L)$, we see that π_m satisfies the steady-state equations

$$0 = v_+ \frac{\partial \pi_+}{\partial y} - \alpha_-[\pi_+ - \pi_-], \tag{3.4a}$$

$$0 = -v_- \frac{\partial \pi_-}{\partial y} + \alpha_+[\pi_+ - \pi_-]. \tag{3.4b}$$

with boundary conditions $\pi_-(0) = 0$ and $\pi_+(L) = 1$. Summing equations (3.4*a*) and (3.4*b*) we have

$$0 = \frac{d}{dy}\left(\frac{v_+}{\alpha_-}\pi_+(y) - \frac{v_-}{\alpha_+}\pi_-(y)\right),$$

which implies

$$\frac{v_+}{\alpha_-}\pi_+(y) - \frac{v_-}{\alpha_+}\pi_-(y) = \frac{v_+}{\alpha_-}\pi_+(0).$$

Solving for $\pi_-(y)$

$$\pi_-(y) = \frac{v_+\alpha_+}{v_-\alpha_-}(\pi_+(y) - \pi_+(0)),$$

and substituting into (3.4*a*) yields

$$\frac{\partial \pi_+}{\partial y} + \gamma \pi_+ = \frac{\alpha_+}{v_-}\pi_+(0), \tag{3.5}$$

with boundary condition $\pi_+(L) = 1$. This has the general solution

$$\pi_+(y) = \pi_+(0)e^{-\gamma y}\left[1 - \frac{\alpha_+}{v_-\gamma}(1 - e^{\gamma y})\right]. \tag{3.6}$$

In particular,

$$\pi_+(0) = \frac{e^{\gamma L}}{1 - \alpha_+[1 - e^{\gamma L}]/v_-\gamma}. \tag{3.7}$$

It also follows that the conditional probability of the vesicle hitting $x = L$ after finite time t without reaching zero, is

$$\mathbb{P}[t < T_m(y)|T_m(y) < \infty] = \frac{\Pi_m(y,t)}{\Pi_m(y,0)}.$$

Thus the conditional MFPT satisfies

$$\omega_m(y) := \mathbb{E}[T_m(y)|T_m(y) < \infty] = \int_0^\infty \frac{\Pi_m(y,t)}{\Pi_m(y,0)}dt,$$

by integrating by parts. Integrating (3.3*a*) and (3.3*b*) with respect to t then gives

$$-\pi_+ = v_+\frac{\partial \pi_+\omega_+}{\partial y} - \alpha_-[\pi_+\omega_+ - \pi_-\omega_-], \tag{3.8a}$$

$$-\pi_- = -v_-\frac{\partial \pi_-\omega_-}{\partial y} + \alpha_+[\pi_+\omega_+ - \pi_-\omega_-], \tag{3.8b}$$

with boundary conditions $\pi_-(0)\omega_-(0) = \pi_+(L)\omega_+(L) = 0$.

Note that a similar analysis can be carried out for exit through the source end at $x = 0$. We denote the corresponding splitting probability and conditional MFPT by $\overline{\pi}_m(y)$ and $\overline{\omega}_m(y)$, respectively. Their explicit solutions for the various splitting probabilities and conditional MFPTs are in [14]. In particular, we have the following probability conservation

$$\pi_m(y) + \overline{\pi}_m(y) = 1. \tag{3.9}$$

3.2. MFPT with nucleation and multiple targets

We now consider the full FPT problem involving multiple cytonemes of different lengths L_k, see Fig. 3. We will simply add a superscript to the above splitting probabilities and MFPTs: $\pi_m^k(y), \omega_m^k(y), \overline{\pi}_m^k(y), \overline{\omega}_m^k(y)$, indicating that $L = L_k$. We

also now include the sticky boundary at $x = 0$ and impose the sticky boundary condition (2.5), see Fig. 4(b). Consider the set of FPTs

$$\begin{aligned}
\mathcal{T}_k &= \inf\{t > 0; X(t) = L_k, N(t) = +, K(t) = k\},\\
\overline{\mathcal{T}}_k &= \inf\{t > 0; X(t) = 0, N(t) = -, K(t) = k\},\\
\overline{\mathcal{T}} &= \inf\{t > 0; X(t) = 0, N(t) = -\}\\
\mathcal{R}_k &= \inf\{t > 0; X(\overline{\mathcal{T}} + t) = L_k, N(\overline{\mathcal{T}} + t) = +, K(\overline{\mathcal{T}} + t) = k\},
\end{aligned}$$

for $k = 1, \cdots, K_T$, where we have suppressed that the morphogen vesicle is initially positioned at the source cell. Next we introduce the sets

$$\Omega_k = \{\mathcal{T}_k < \infty\}, \quad \Gamma_k = \{\overline{\mathcal{T}}_k = \overline{\mathcal{T}} < \infty\}, \quad \Gamma = \{\overline{\mathcal{T}} < \infty\}.$$

In other words, Ω_k is the set of all events for which the motor cargo eventually delivers the morphogen vesicle to the kth target cell mediated by the kth cytoneme. It immediately follows that

$$\Omega_k \backslash \Gamma = \{\mathcal{T}_k < \overline{\mathcal{T}} = \infty\}.$$

That is, $\Omega_k \backslash \Gamma$ is the set of all events for which the motor cargo delivers the morphogen vesicle to the kth target cell without any nucleation. Moreover, since $\overline{\mathcal{T}} = \inf_{k'} \overline{\mathcal{T}}_{k'}$, then $\Omega_k \cap \Gamma_{k'}$ are mutually disjoint with respect to k'. Thus we have

$$\Omega_k \cap \Gamma = \bigcup_{k'} \Omega_k \cap \Gamma_{k'} = \bigcup_{k'} \{\overline{\mathcal{T}}_{k'} = \overline{\mathcal{T}} < \mathcal{T}_k < \infty\}.$$

This means that $\Omega_k \cap \Gamma$ is decomposed as the union of $\Omega_k \cap \Gamma_{k'}$, which is the set of all events for which the motor cargo is initially injected to the k'th cytoneme and then eventually delivers the morphogen vesicle to the kth target cell.

In order to deal with the nucleation effect connecting multiple cytonemes, we will proceed along similar lines to [5] by using the strong Markov property. First, the splitting probability ρ_k of delivery into the kth target cell, starting at the source cell, can be decomposed as

$$\begin{aligned}
\rho_k &= \mathbb{P}[\Omega_k] = \mathbb{P}[\Omega_k \backslash \Gamma] + \mathbb{P}[\Omega_k \cap \Gamma]\\
&= \theta_k \cdot \pi_+^k(0) + \mathbb{P}[\Omega_k \cap \Gamma]\\
&= \theta_k \cdot \pi_+^k(0) + \sum_{k'} \mathbb{P}[\Omega_k \cap \Gamma_{k'}].
\end{aligned} \tag{3.10}$$

Moreover,

$$\begin{aligned}
\mathbb{P}[\Omega_k \cap \Gamma_{k'}] &= \mathbb{P}[\Gamma_{k'}] \cdot \mathbb{P}[\mathcal{R}_k < \infty]\\
&= \theta_{k'}[1 - \pi_+^{k'}(0)] \cdot \mathbb{P}[\mathcal{R}_k < \infty].
\end{aligned}$$

The strong Markov property yields that

$$\mathbb{P}[\Omega_k \cap \Gamma_{k'}] = \rho_k \cdot \theta_{k'}[1 - \pi_+^{k'}(0)], \tag{3.11}$$

according to the probability conservation (3.9). Substituting (3.11) into (3.10) and rearranging we have

$$\rho_k = \frac{\theta_k \pi_+^k(0)}{\sum_{k'} \theta_{k'} \pi_+^{k'}(0)}. \tag{3.12}$$

Next, we introduce the MFPT $z_k := \mathbb{E}[\mathcal{T}_k 1_{\Omega_k}]$, which decomposed as

$$\begin{aligned} z_k &= \mathbb{E}[\mathcal{T}_k 1_{\Omega_k \setminus \Gamma}] + \mathbb{E}[\mathcal{T}_k 1_{\Omega_k \cap \Gamma}] \\ &= \theta_k \pi_+^k(0) \cdot \left[\frac{1}{r_0} + \omega_+^k(0)\right] + \mathbb{E}[(\overline{\mathcal{T}} + \mathcal{R}_k) 1_{\Omega_k \cap \Gamma}] \\ &= \theta_k \pi_+^k(0) \cdot \left[\frac{1}{r_0} + \omega_+^k(0)\right] + \sum_{k'} \mathbb{E}[\overline{\mathcal{T}}_{k'} | \Omega_k \cap \Gamma_{k'}] \mathbb{P}[\Omega_k \cap \Gamma_{k'}] \\ &\quad + \mathbb{E}[\mathcal{R}_k 1_{\Omega_k \cap \Gamma}]. \end{aligned}$$

Again involving the strong Markov property gives that the conditional MFPT to be captured by the kth target cell is z_k/ρ_k. Thus we have

$$\begin{aligned} z_k &= \theta_k \pi_+^k(0) \cdot \left[\frac{1}{r_0} + \omega_+^k(0)\right] + \sum_{k'} \left[\frac{1}{r_0} + \overline{\omega}_+^{k'}(0)\right] \cdot \rho_k \theta_{k'} [1 - \pi_+^{k'}(0)] \\ &\quad + \frac{z_k}{\rho_k} \cdot \rho_k \sum_{k'} \theta_{k'} [1 - \pi_+^{k'}(0)]. \end{aligned}$$

Rearranging the above equation and using (3.12) we therefore find that the conditional MFPT is

$$\tau_k \equiv \frac{z_k}{\rho_k} = \left[\frac{1}{r_0} + \omega_+^k(0) + \sum_{k'} \rho_{k'} \frac{\overline{\pi}_+^{k'}(0)}{\pi_+^{k'}(0)} \left[\frac{1}{r_0} + \overline{\omega}_+^{k'}(0)\right]\right]. \tag{3.13}$$

4. Impulsive signaling by periodically generated vesicles

In sections 2 and 3 we focused on the transport of a single vesicle along cytonemes, without specifying what happens after a vesicle is captured by a target cell. Once a vesicle is captured by a target cell, it delivers a certain amount of morphogen to the target cell. We will refer to this as a morphogen "burst" so that the discrete nature of vesicular transport can be treated as an impulsive signal. The transport of multiple vesicles generated by the source cell thus results in multiple impulsive signals that ultimately form a morphogen gradient. For simplicity, we assume that the source cell produces a morphogen vesicle with constant frequency ν. We also take the amount of morphogen transported by a vesicle to be of fixed size Δ. (Note that $Q := \nu\Delta$ is the average morphogen production rate in the source cell.)

Following section 3, if a vesicle is produced by the source cell, then the probability that a single impulsive signal reaches the kth target cell is ρ_k and the conditional MFPT for the event is τ_k. The other $K_T - 1$ target cells do not receive any morphogen. Now suppose that the source cell generates an impulsive signal periodically. Let $i = 1, 2, \cdots$ label the ordered sequence of vesicles produced by the source cell, and denote the target cell that receives the ith vesicle by k_i. If $\mathcal{B}_i$ is the bursting or capture time of the ith vesicle, then

$$\mathcal{B}_i = \frac{1}{\nu}(i-1) + \mathcal{T}_{k_i}. \tag{4.1}$$

We also denote the random identity of the cell that captures the vesicle by $\mathcal{K}$.

Consider a specific target cell $k = \bar{k}$. This cell receives a morphogen burst of size Δ at time $\mathcal{B}_i$ if $k_i = \bar{k}$, otherwise it receives nothing. Furthermore, suppose that morphogen delivered to the target cell degrades at a rate κ. We would like to determine the steady-state amount of morphogen within the target cell in the long

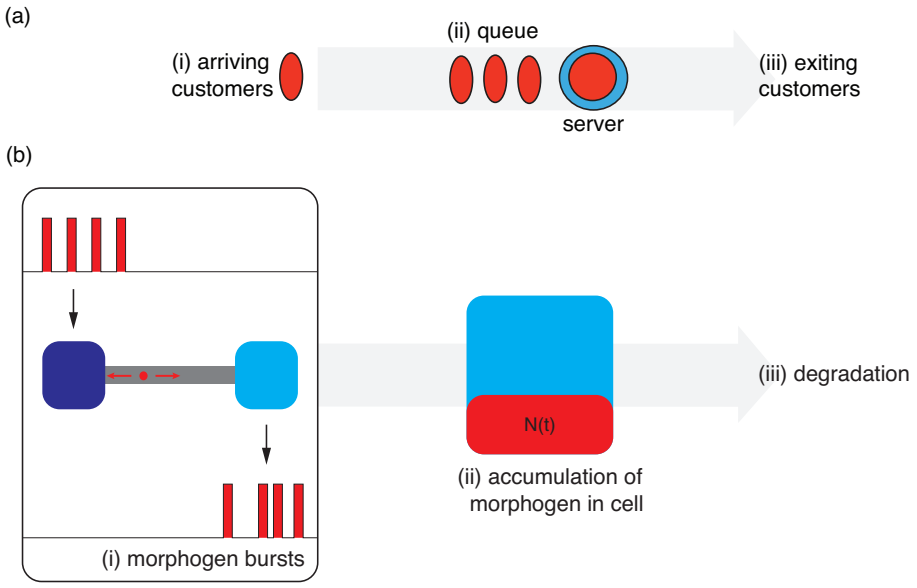

Figure 5: Queuing theory and impulsive signaling transport. (a) Example of a single-server queue. (b) Impulsive signals. Periodically formed morphogen vesicles in the source cell generate a random sequence of impulsive signals within a target cell. This is analogous to an infinite-server queuing model.

time limit. We will proceed by reformulating the multiple impulsive signaling model as a queuing process, see Fig. 5, analogous to the study of search-and-capture model of morphogen gradient formation in vertebrates [5].

Queuing theory concerns the mathematical analysis of waiting lines formed by customers randomly arriving at some service station and staying in the system until they receive service from a group of servers. Different types of queuing process are defined in terms of (i) the stochastic process underlying the arrival of customers, (ii) the distribution of the number of customers (batches) in each arrival, (iii) the stochastic process underlying the departure of customers (service-time distribution), and (iv) the number of servers. Our impulsive signaling transport model can be matched into a queuing process as follows: Individual vesicles are analogous to customers, morphogen bursts correspond to customers arriving in batches, and the degradation of morphogens is the analog of customers exiting the system after service. It follows that the waiting time distribution of morphogen degradation corresponds to the service time distribution. Since the morphogens are degraded independently of each other, the effective number of servers in the corresponding queuing model is infinite.

In previous work, we mapped a search-and-capture model of cytoneme-based morphogenesis in vertebrates to a $G/M/\infty$ queue [5] . Here the symbol G denotes a general interarrival time, the symbol M stands for a Markovian (or exponential) service time distribution $E(t) = 1 - e^{-\kappa t}$ for morphogen degradation, and ∞ denotes infinite servers. However, in our current model there is no guarantee that a vesicle produced earlier arrives at a target cell before a vesicle produced later. That is,

the condition $\mathcal{B}_i < \mathcal{B}_j$ for $i < j$ need not hold. Thus, one cannot define a positive interarrival time in our impulsive signaling transport model. We solve this issue by introducing an arrival time, instead of an interarrival time, and finding the iterative structure that allows us to use queuing theory. In order to proceed, we need to define the arrival time distribution $F(t,k)$ related to the quantities in section 3. We can write

$$\begin{aligned} F(t,k) &= \mathbb{P}[\mathcal{B} < t, \mathcal{K} = k] = \mathbb{P}[\mathcal{B} < t | \mathcal{K} = k] \cdot \mathbb{P}[\mathcal{K} = k] \\ &= \rho_k \int_0^t f_k(y) dy, \end{aligned} \tag{4.2}$$

where $f_k(y)$ is the density for the conditional MFPT of a single impulsive signaling event that ends at the kth cell. In particular, we have

$$\int_0^\infty y f_k(y) dy = \tau_k, \tag{4.3}$$

with τ_k given by equation (3.13).

Let $N(t)$ be the number of waiting customers at time t. This corresponds to the number of morphogens in the labeled target cell $\bar{k}$ that have not yet degraded. In terms of the sequence of arrival times (morphogen bursting times) $\mathcal{B}_i$ and cell identities k_i, one can write

$$N(t) = \sum_{j \geq 1, (j-1)/\nu \leq \mathcal{B}_j \leq t} \chi(t - \mathcal{B}_j) \delta_{k_j, \bar{k}} \tag{4.4}$$

where

$$\chi(t - \mathcal{B}_j) = \sum_{d=1}^{\Delta} I(t - \mathcal{B}_j, S_{jd}) \tag{4.5}$$

for

$$I(t - \mathcal{B}_j, S_{jd}) = \begin{cases} 0 & \text{if } t - \mathcal{B}_j < 0 \\ 1 & \text{if } 0 \leq t - \mathcal{B}_j \leq S_{jd} \\ 0 & \text{if } t - \mathcal{B}_j > S_{jd} \end{cases} . \tag{4.6}$$

Here S_{jd}, $d = 1, \ldots, \Delta$, is the service time of the dth member of a burst delivered to the cell $\bar{k}$. We will assume that the system is empty at time $t = 0$ ($N(0) = 0$).

The moments of the queuing process can be determined using generating functions and Laplace transforms. Since the analysis is quite involved, we leave the details to appendix A. Here we simply write down the expressions for the steady-state mean and variance, under the assumption that all moments of $F(y, \bar{k})$ are finite. In particular,

$$\begin{aligned} \langle N \rangle &= \frac{\Delta}{\kappa} \lim_{s \to 0} \frac{\widehat{f}(s, \bar{k})}{1 - e^{-s/\nu}} = \frac{\nu \Delta}{\kappa} \rho_{\bar{k}} \\ &= \frac{Q}{\kappa} \rho_{\bar{k}}, \end{aligned} \tag{4.7}$$

and

$$\langle N^2 \rangle - \langle N \rangle^2 = \langle N \rangle \left[\frac{3 + \Delta}{4} - \rho_{\bar{k}} \mathcal{I}_{\bar{k}}(\kappa) \Delta \right], \tag{4.8}$$

where

$$\mathcal{I}_{\bar{k}}(\kappa) = \int_0^\infty e^{-\kappa y'} \int_0^\infty f_{\bar{k}}(y) f_{\bar{k}}(y + y') dy dy'. \tag{4.9}$$

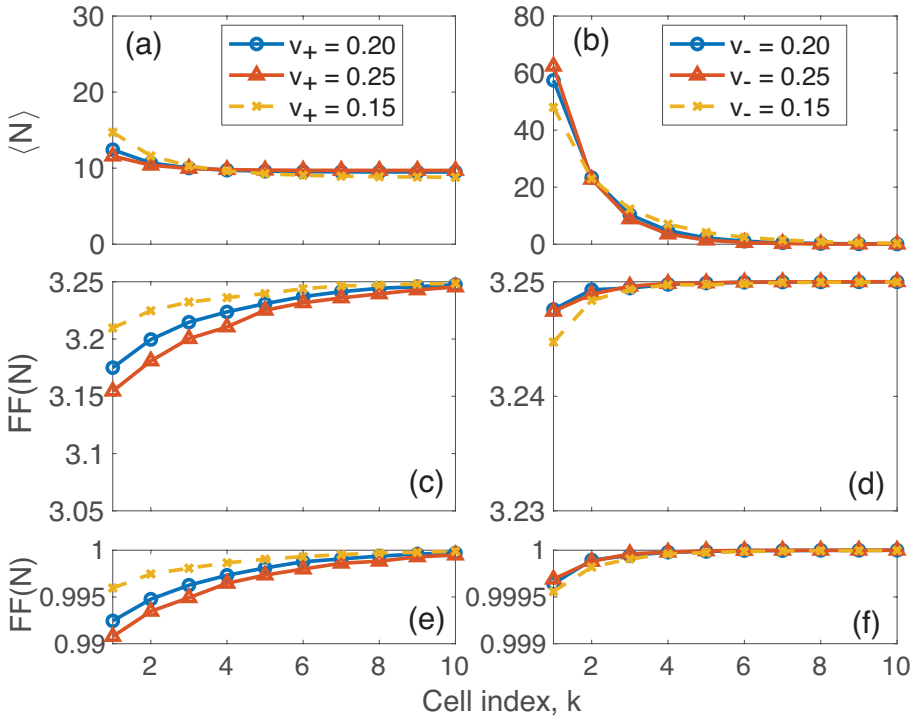

Figure 6: Steady-state mean and variance of $N(t)$ for various transport speed values. (a) First moments of anterograde-dominant case ($\bar{v} > 0$) with various v_+ and $v_- = 0.1\mu m/s$. (b) First moments of retrograde-dominant case ($\bar{v} < 0$) with $v_+ = 0.1\mu m/s$ and various v_-. (c,d) Corresponding plots of the Fano factor when $\Delta = 10$ and $\nu = 0.5/s$. (e,f) Corresponding plots of the Fano factor when $\Delta = 1$ and $\nu = 5/s$. Injection probability θ_k is uniformly distributed. Parameters are as follows: $\alpha_\pm = 0.1/s$, $r_0 = 0.05/s$, $K_T = 10$, $\kappa = 0.05/s$, $Q = 5/s$.

The corresponding Fano factor (FF) is

$$\mathrm{FF}_N = \frac{\langle N^2\rangle - \langle N\rangle^2}{\langle N\rangle} = 1 + \left[\frac{\Delta - 1}{4} - \rho_{\bar{k}}\mathcal{I}_{\bar{k}}(\kappa)\Delta\right], \tag{4.10}$$

which is independent of the vesicle production rate ν. Since $\rho_k \leq 1$ and $\mathcal{I}_k \leq 1/2$ (see below), it follows that for all k

$$\frac{3-\Delta}{4} \leq \mathrm{FF}_N \leq \frac{\Delta+3}{4}. \tag{4.11}$$

Recall that the Fano factor of a Poisson process is $\mathrm{FF}_{\mathrm{Poiss}} = 1$ so that $\mathrm{FF}_N \leq \mathrm{FF}_{\mathrm{Poiss}}$ when $\Delta = 1$. We also find that FF_N is only weakly dependent on k, which means that relative fluctuations are particularly significant for distal target cells. Note that one can reduce the relative size of fluctuations for fixed Δ and κ by increasing the production rate ν, as FF_N is independent of ν.

We now explore in more detail how the mean $\langle N\rangle$ and Fano factor FF_N vary with distance L_k of the target cell from the source cell. For the moment, assume that the probability of allocating a vesicle to a particular cytoneme is uniform, $\theta_k = 1/K_T$.

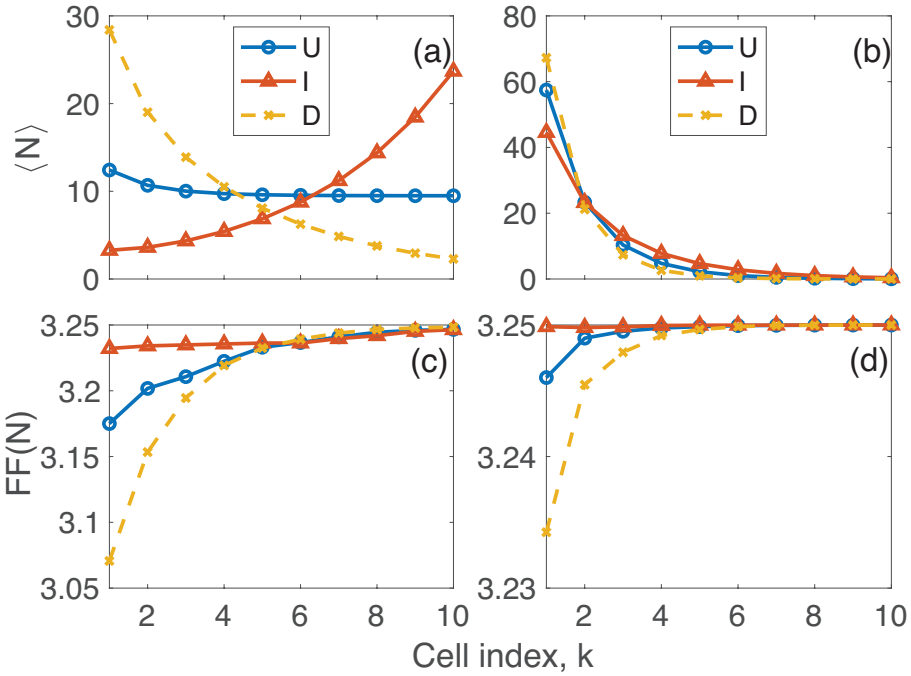

Figure 7: Moments of steady-state distribution of $N(t)$ for three different injection distributions: a uniform distribution θ_k^U, a monotone increasing distribution θ_k^I and a monotone decreasing distribution θ_k^D. (a) First moments of anterograde-dominant case ($\bar{v} > 0$) with $v_+ = 0.2\mu m/s$ and $v_- = 0.1\mu m/s$ for various injection distributions. (b) Corresponding first moments of retrograde-dominant case ($\bar{v} < 0$) with $v_+ = 0.1\mu m/s$ and $v_- = 0.2\mu m/s$. (c,d) Corresponding plots of the Fano factor when $\Delta = 10$ and $\nu = 0.5/s$. Other parameters are the same as in Fig. 6.

Numerical results in Fig. 6(a,b) show that the behavior of steady-state mean $\langle N \rangle$ is determined by the sign of $\bar{v}$, which is the average transport speed

$$\bar{v} = v_+ \frac{\alpha_+}{\alpha_+ + \alpha_-} - v_- \frac{\alpha_-}{\alpha_+ + \alpha_-}.$$

If the transport is dominated by the anterograde state ($\bar{v} > 0$), then the asymptotic value converges to a non-zero value so that the morphogen gradient is almost flat with respect to the distance of target cell. On the other hand, if the transport is dominated by the retrograde state ($\bar{v} < 0$), then the asymptotic value decays to zero. We thus recover the results of our previous work on a "fluid" model [4]. Fig. 6(c,d) illustrates the additional features of our stochastic model, namely, that the Fano factor can be greater than one (non-Poissonian) and is approximately constant along the length of the array of target cells. That is, relative fluctuations are particularly significant in the case of distal target cells and $\bar{v} < 0$.

Following along similar lines to our previous deterministic model [4], we can also investigate the affects of non-uniform resource allocation. In particular, we consider

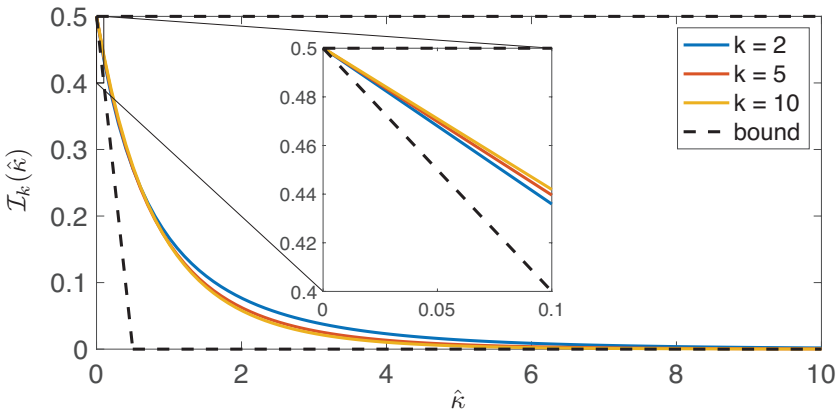

Figure 8: Dimensionless function $\mathcal{I}_k(\hat{\kappa})$ for various k when the transport is anterograde-dominant ($\bar{v} > 0$). Parameters as Fig. 6. Similar results hold when $\bar{v} < 0$.

three different injection distributions:

$$\theta_k^U = \frac{1}{K_T}, \quad \theta_k^I = \frac{e^{k/4}}{\mathcal{N}_I}, \quad \theta_k^D = \frac{e^{(K_T+1-k)/4}}{\mathcal{N}_D}, \quad k = 1, 2, \cdots, K_T,$$

which represents a uniform distribution, a monotone increasing distribution, and a monotone decreasing distribution, respectively. Here $\mathcal{N}_{I,D}$ are normalization constants. Numerical results in Fig. 7 show that the anterograde-dominant distribution of $\langle N \rangle$ is more sensitive to the choice of the injection distribution. The numerics are obtained by using the splitting probability (3.12) and the MFPT (3.13) of a single particle and the numerical results for $\mathcal{I}_k$ (see below).

The k-dependence of FF_N is determined by the splitting probability ρ_k and the dimensionless function $\mathcal{I}_{\bar{k}}(\kappa)$. It turns out that the latter is only weakly dependent on the target cell index k, and can be bounded. In order to non-dimensionalize the integral variables, we substitute $y = \tau_{\bar{k}}\xi$ and $y' = \tau_{\bar{k}}\eta$

$$\mathcal{I}_{\bar{k}}(\hat{\kappa}) = \mathcal{I}_{\bar{k}}(\kappa) = \int_0^\infty \int_0^\infty e^{-\hat{\kappa}\xi} g(\xi+\eta) g(\eta) d\xi d\eta, \tag{4.12}$$

where $\hat{\kappa} = \kappa\tau_{\bar{k}}$ and $g(\xi) = \tau_{\bar{k}} f_{\bar{k}}(\tau_{\bar{k}} y)$ so that

$$\int_0^\infty g(\xi) d\xi = 1, \quad \int_0^\infty \xi g(\xi) dx = 1.$$

Since $1 - \hat{\kappa}\xi \le e^{-\hat{\kappa}\xi} \le 1$, then one can bound

$$\mathcal{J}_0 - \kappa \mathcal{J}_1 \le \mathcal{I}_{\bar{k}}(\hat{\kappa}) \le \mathcal{J}_0$$

where

$$\mathcal{J}_0 = \int_0^\infty \int_0^\infty g(\xi+\eta) g(\eta) d\xi d\eta, \quad \mathcal{J}_1 = \int_0^\infty \int_0^\infty \xi g(\xi+\eta) g(\eta) d\xi d\eta.$$

After integration, we have

$$\mathcal{J}_0 = \int_0^\infty g(\eta) \int_\eta^\infty g(\xi) d\xi d\eta = -\frac{1}{2} \int_0^\infty \frac{d}{d\eta} \left[\int_\eta^\infty g(\xi) d\xi \right]^2 d\eta = \frac{1}{2}. \tag{4.13}$$

Another change of variables and integration gives

$$\mathcal{J}_1 = \int_0^\infty \int_\eta^\infty (\xi - \eta) g(\xi) g(\eta) d\xi d\eta = 2 \int_0^\infty \int_\eta^\infty \xi g(\xi) g(\eta) d\xi d\eta - 1 < 1. \tag{4.14}$$

Together with (4.13) and (4.14) it follows that

$$\frac{1}{2} \geq \mathcal{I}_{\bar{k}}(\hat{\kappa}) > \max\left\{\frac{1}{2} - \hat{\kappa}, 0\right\}, \tag{4.15}$$

in accordance with the positivity of $\mathcal{I}_{\bar{k}}(\hat{\kappa})$. In particular, if $\hat{\kappa} \ll 1$ so that $\tau_{\bar{k}} \ll \frac{1}{\kappa}$, which means that the degradation time is much slower than the arrival time from the source cell to the kth target cell, then $\mathcal{I}_{\bar{k}}(\hat{\kappa}) \sim 1/2$. On the other hand, if $1 \ll \hat{\kappa}$, then $\lim_{\hat{\kappa}\to\infty} \mathcal{I}_{\bar{k}}(\hat{\kappa}) = 0$. Numerical results in Fig. 8 confirm the asymptotic behavior of $\mathcal{I}_k$ and the analytic result that the dimensionless function is bounded by the inequality (4.15). The numerics are obtained by carrying out a Monte Carlo integration of (4.12) and generating samples of the conditional distribution g using the Gillespie algorithm. The weak dependence on the index k is clearly seen.

One final observation regarding the steady-state distribution is that the first moment $\langle N \rangle$ in (4.7) does not explicitly depend on the conditional MFPT τ_k. For the search-and-capture model in [5], the mean steady-state distribution of morphogens in a cell depends on the conditional MFPT because the interarrival time is determined by the FPTs. However, in the present case, the interarrival time is

$$\mathcal{B}_{i+1} - \mathcal{B}_i = \frac{1}{\nu} + \mathcal{T}_{k_{i+1}} - \mathcal{T}_{k_i},$$

which expectation is the vesicle production time $1/\nu$. Therefore, the first moment of the impulsive signaling transport depends on the vesicle production rate ν, rather than the MFPTs.

5. Differential version of impulsive signaling transport

In this section we relate our impulsive signaling model with the "fluid" transport model of [4, 10]. We proceed by constructing a differential version of the former model, and then deriving the "fluid" transport model by homogeniziation..

Consider the ith vesicle injected into a single cytoneme of length L. Let $p_n(x,t,i)$ be the probability density that the vesicle is positioned at x in state $n \in \{+,-\}$ at time t. This satisfies the same differential CK equations (2.1*a*) and (2.1*b*) with the boundary conditions (2.2). Here $P_0(t,i)$ is the probability that the vesicle is located in the source cell at time t, which evolves according to

$$\frac{dP_0}{dt}(t,i) = \delta(t - (i-1)/\nu) + v_- p_-(0,t,i) - r_0 P_0(t,i), \tag{5.1}$$

where $\delta(t)$ is the Dirac delta function. Once the vesicle reaches the right-hand end at $x = L$, morphogens in the vesicle burst into the target cell and subsequently degrade. Let $Q_d(t,i)$ be the probability that the dth morphogen is in the target cell, which satisfies

$$\frac{dQ_d(t,i)}{dt} = v_+ p_+(L,t,i) - \kappa Q_d(t,i), \quad d = 1, 2, \cdots, \Delta. \tag{5.2}$$

Introducing the mean number of morphogen in the target cell,

$$C_1(t) := \sum_{i=1}^{\infty} \sum_{d=1}^{\Delta} Q_d(t,i),$$

and summing equations (5.1) and (5.2) with respect to i, d yields

$$\frac{dC_0}{dt} = \mathcal{Q}(t) + v_- u_-(L,t) - r_0 C_0(t), \tag{5.3a}$$

$$\frac{dC_1}{dt} = v_+ u_+(L,t) - \kappa C_1(t), \tag{5.3b}$$

where

$$\mathcal{Q}(t) = \Delta \sum_{i=1}^{\infty} \delta(t - (i-1)/\nu), \tag{5.4}$$

and $u_\pm(x,t)$ satisfies the following equations over $(0, L)$

$$\frac{\partial u_+}{\partial t} = -v_+ \frac{\partial u_+}{\partial x} - \alpha_- u_+ + \alpha_+ u_-, \tag{5.5a}$$

$$\frac{\partial u_-}{\partial t} = v_- \frac{\partial u_-}{\partial x} + \alpha_- u_+ - \alpha_+ u_-, \tag{5.5b}$$

together with the boundary conditions

$$v_+ u_+(0,t) = r_0 C_0(t), \quad u_-(L,t) = 0. \tag{5.6}$$

Once can interpret $\mathcal{Q}(t)$ as the average time-dependent production rate. In particular, when $\kappa \ll \nu$, which means that the production period is much shorter than the average degradation time, the production rate can homogenized as

$$\mathcal{Q}(t) \approx Q \int_0^{\infty} \delta(t - t')dt' = Q. \tag{5.7}$$

This homogenized model is exactly same asthe "fluid" transport model in [4, 10], which means that the model is an asymptotic model of impulsive signaling model when the production rate is faster than the degradation model.

One can extend the above result for multiple cytonemes. In the same fashion, one determines the average number of morphogen in the kth target cell $C_k(t)$ satisfying

$$\frac{dC_0}{dt} = \mathcal{Q}(t) - r_0 C_0(t) + v_- \sum_{k=1}^{K_T} u_-^k(L,t), \tag{5.8a}$$

$$\frac{dC_k}{dt} = v_+ u_+^k(L_k,t) - \kappa C_k(t), \tag{5.8b}$$

where $u_\pm^k(x,t)$ satisfies (5.5a) and (5.5b) over $(0, L_k)$ with boundary conditions

$$v_+ u_+^k(0,t) = r_0 \theta_k C_0(t), \quad u_-^k(L,t) = 0. \tag{5.9}$$

One major result from the fluid model is the steady-state concentration of morphogen in a target cell. For the kth target cell, the steady-state concentration takes the form of

$$C_k^* = \frac{Q}{\kappa} \frac{\theta_k w(L_k)}{\sum_{k'=1}^{K_T} \theta_{k'} w(L_{k'})}, \tag{5.10}$$

where

$$w(x) = \frac{e^{\gamma x}}{1 + \alpha_+[1 - e^{\gamma x}]/\gamma v_-}, \quad \gamma = \frac{\alpha_+ v_+ - \alpha_- v_-}{v_+ v_-}. \tag{5.11}$$

Comparing with the steady-state mean number of morphogen derived by the impulsive signaling model (4.7), they are identical if

$$\pi_+^k(0) = w(L_k).$$

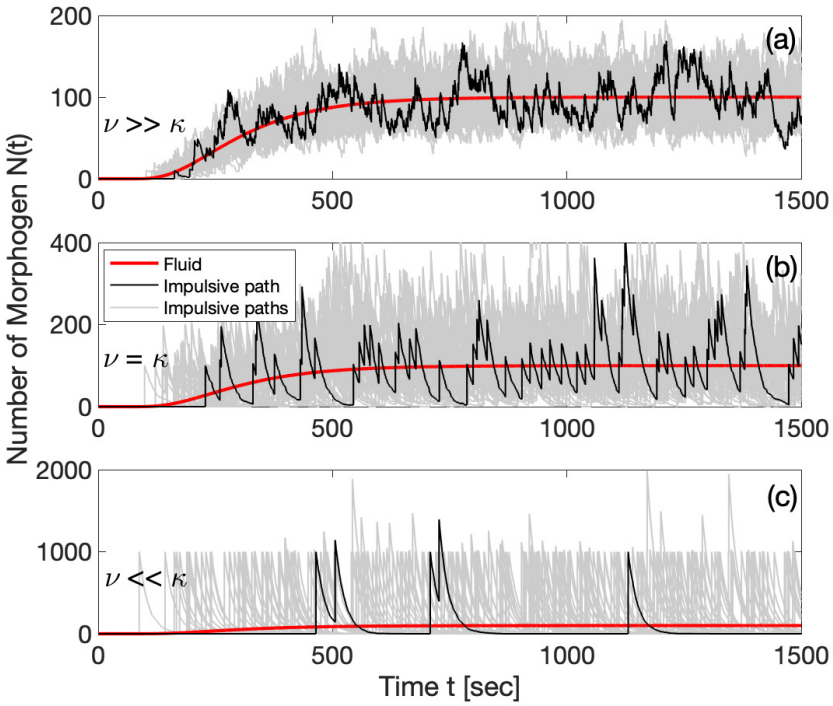

Figure 9: "Fluid" model (solid and red) gives the average dynamics of the impulsive signaling model. (a) Sample paths of the impulsive signaling model of a single cytoneme when $\nu = 10\kappa$. (b) Corresponding plot when $\nu = \kappa$. (b) Corresponding plot when $\nu = 0.1\kappa$. Parameters are the same as Fig. 6 with $\kappa = 0.05/s$ and fixed $Q = 5/s$.

Comparing with equation (3.7) for $L = L_k$,we see that $\pi_+^k(0) = w(L_k)$. This proves that the steady-state solution of the fluid model and the steady-state mean of the impulsive signaling model are the same, which can be confirmed numerically as illustrated in Fig. 9.

6. Discussion

In this paper we developed a stochastic model of cytoneme-based morphogenesis, where individual vesicles of morphogen are bidirectionally transported along cytonemes linking a source cell to one or more target cells. We calculated the splitting probabilities and the conditional MFPTs of a single vesicle delivering a morphogen burst to a target cell, and then used queuing theory to determined the steady-state mean and variance of the morphogen gradient, assuming that morphogen vesicles are periodically generated by the source cell. We also developed a differential version of the queuing model and showed that the continuum model of cytoneme-based morphogenesis [4, 10] is the asymptotic mean dynamics of the queuing model when the degradation rate is faster than the vesicle production rate.

One of the major results of our stochastic model is that the burst-like nature of morphogen transport can lead to a Fano factor that is greater than unity (non-Poissonian), analogous to protein bursting in gene networks [13]. Moreover, the Fano factor is only weakly-dependent on distance between the source and target cells, which means that relative fluctuations could be particularly significant in the case of target cells distal to the source cells. On way to mitigate the affects of fluctuations is to increase the production rate relative to the degradation rate.

One simplifying assumption of our stochastic model is that vesicles are periodically produced in the source cell at a constant rate ν and contain the same amount of morphogen. However, fluctuations in the production rate and size of vesicles could be an additional source of stochasticity, resulting in a queuing model with random customer batch sizes and more complicated waiting time distributions. Another assumption is that the injection probability θ_k is time-independent. However, this probability depends on the relative number of cytonemes connecting to each target cell. Recent experimental studies of gradient formation of a FGF family protein, Branchless (Bnl), in *Drosophila* have shown that the number of cytonemes can be time-dependent [6, 20]. In Drosophila, Bnl is the primary signal that guides the branching morphogenesis of tracheal epithelial tubes in the wing imaginal disc. Activation of its cognate receptor Breathless (Btl) in tracheoblast cells induces migration and remodeling of the tracheoblasts to form a new tubular branch, the Air-Sac-Primordium (ASP). ASP cells extend Btl-containing cytonemes to contact the basal surface of the wing disc source and directly receive Bnl. The latter regulates Btl synthesis and cytoneme production via a feedback loop that helps sculpt the morphogen gradient. Thus the number of cytoneme contacts, which determines θ_k, is itself a dynamical variable.

Appendix

In this appendix, we use generating functions and Laplace transforms to derive expressions for the steady-state mean and variance of the modified G/M/∞ queuing model. First, we define the binomial moments

$$B_r(t) = \sum_{l=r}^{\infty} \frac{l!}{(l-r)!r!} \mathbb{P}[N(t) = l], \quad r = 1, 2, \cdots. \tag{A.1}$$

Introducing the generating function

$$G(z,t) = \sum_{l=0}^{\infty} z^l \mathbb{P}[N(t) = l], \tag{A.2}$$

we have

$$B_r(t) = \frac{1}{r!} \left. \frac{d^r G(z,t)}{dz^r} \right|_{z=1}. \tag{A.3}$$

Assuming that the system is empty at time $t = 0$, we will derive an integral equation for the generating function $G(z,t)$. Rearranging (4.4) we have

$$N(t) = \chi(t - \mathcal{B}_1)\delta_{k_1,\bar{k}} + H(t - 1/\nu)N^*(t - 1/\nu), \tag{A.4}$$

where $N^*(t)$ has the same distribution as $N(t)$. Note that $\chi(t - \mathcal{B}_1)\delta_{k_1,\bar{k}}$ and $H(t - 1/\nu)N^*(t - 1/\nu)$ are independent. Conditioning the first arrival time $\mathcal{B}_1 =$

$\mathcal{T}_{k_1} = y$ and cell identity $k_1 = k$, one has

$$\begin{aligned} g(z,t,y,k) &\equiv \mathbb{E}[z^{N(t)}|\mathcal{B}_1 = y, k_1 = k] \\ &= \mathbb{E}[z^{H(t-1/\nu)N^*(t-1/\nu)}]\mathbb{E}[z^{\chi(t-y),\delta_{k,\bar{k}}}|\mathcal{B}_1 = y, k_1 = k]. \end{aligned} \tag{A.5}$$

Moreover,

$$\mathbb{P}[I(t-y, S_{1d}) = l] = [1 - E(t-y)]\delta_{l,1} + E(t-y)\delta_{l,0},$$

so it follows that

$$\sum_{l=0,1} z^l \mathbb{P}[I(t-y, S_{1d}) = l] = z + (1-z)E(t-y),$$

where $t - y > 0$. Since $I(t-y, S_{1d})$ for $d = 1, 2, \cdots, \Delta$ are independent and identically distributed, the total expectation theorem yields

$$\begin{aligned} G_2(z,t) &:= \mathbb{E}[z^{\chi(t-\mathcal{B}_1)\delta_{k_1,\bar{k}}}] = \mathbb{E}\left[\mathbb{E}[z^{\chi(t-\mathcal{B}_1)\delta_{k_1,\bar{k}}}|\mathcal{B}_1 = y, k_1 = k]\right] \\ &= \mathbb{E}\left[\prod_{d=1}^{\Delta} \mathbb{E}[z^{\delta_{k,\bar{k}} I(t-y,S_{1d})}]\right] \\ &= \int_0^t [z + (1-z)E(t-y)]^{\Delta} dF(y,\bar{k}) + \int_t^{\infty} dF(y,\bar{k}) + \sum_{k\neq\bar{k}} \rho_k. \end{aligned}$$

According to (A.5), another application of the total expectation theorem gives

$$\begin{aligned} G(z,t) &= \mathbb{E}[z^{N(t)}] = \mathbb{E}[g(z,t,y,k)] \\ &= \mathbb{E}[z^{H(t-1/\nu)N^*(t-1\nu)}] \cdot \mathbb{E}\left[\mathbb{E}[z^{\chi(t-y),\delta_{k,\bar{k}}}|\mathcal{B}_1 = y, k_1 = k]\right] \\ &= G_1(z, t-1/\nu) \times G_2(z,t), \end{aligned} \tag{A.6}$$

where

$$G_1(z, t-1/\nu) = \begin{cases} 1 & \text{if } t < 1/\nu \\ G(z, t-1/\nu) & \text{if } t \geq 1/\nu \end{cases}.$$

One can now obtain an iterative equation for binomial moments by differentiating equation (A.6) with respect to z and using equation (A.3. Since

$$\frac{d^l}{dz^l}[z + (1-z)E(t-y)]^{\Delta}\Big|_{z=1} = \begin{cases} \frac{\Delta!}{(\Delta-l)!}[1 - E(t-y)]^l & \text{if } \Delta \geq l \\ 0 & \text{if } \Delta < l \end{cases},$$

we obtain the integral equation

$$B_r(t) = \binom{\Delta}{r}\mathcal{H}_r(t) + H(t-1/\nu)\sum_{l=0}^{r-1}\binom{\Delta}{l} B_{r-l}(t-1/\nu)\mathcal{H}_l(t) \tag{A.7}$$

where $\mathcal{H}_0(t) = 1$ and

$$\mathcal{H}_l(t) = \int_0^t e^{-\kappa l(t-y)} dF(y,\bar{k}), \quad l = 1, 2, \cdots.$$

In order to obtain the steady-state binomial moments, we Laplace transform equation (A.7) after making the substitution $dF(y,\bar{k}) = \rho_{\bar{k}} f_{\bar{k}}(y)dy$. In particular, for $r = 1$, we have

$$\widehat{B}_1(s) = e^{-s/\nu}\widehat{B}_1(s) + \frac{\Delta}{\kappa + s}\widehat{f}_{\bar{k}}(s).$$

Solving for $\widehat{B}_1(s)$ gives

$$\widehat{B}_1(s) = \frac{\Delta}{\kappa + s} \cdot \frac{\widehat{f}_{\bar{k}}(s)}{1 - e^{-s/\nu}}.$$

Using the fact that $\lim_{t\to\infty} B_1(t) = \lim_{s\to 0} s\widehat{B}_1(s)$ and using l'Hospital's rule, we obtain the expression for steady-state first moment $B_1^* = \langle N \rangle$ given in equation (4.7), assuming that all moments of $F(y, \bar{k})$ are finite.

Note that if $r \geq 2$ then one cannot perform Laplace transforms directly to find an iterative equation for the steady-state binomial moments. This is due to the presence of terms involving products of time-dependent functions. Therefore, in order to determine the steady-state second binomial moment, we introduce an iterative expression for the moment generating function:

$$G(z,t) = \prod_{j=0}^{i-1} G_2(z, t - j/\nu), \quad i - 1 \leq t\nu < i. \tag{A.8}$$

Differentiating with respect to z we have

$$\frac{dG}{dz}(z,t) = G(z,t) \sum_{j=0}^{i-1} \frac{1}{G_2} \frac{dG_2}{dz}\bigg|_{z,t-j/\nu}.$$

Again taking derivatives with respect to z

$$\frac{d^2G}{dz^2}(z,t) = \left[\frac{dG}{dz}\right]^2 \frac{1}{G}\bigg|_{z,t} + \sum_{j=0}^{i-1} \frac{1}{G_2}\frac{d^2G_2}{dz^2} - \frac{1}{G_2^2}\left[\frac{dG_2}{dz}\right]^2\bigg|_{z,t-j/\nu}$$

and setting $z = 1$ yields

$$B_2(t) = \frac{1}{2}B_1^2(t) + \binom{\Delta}{2} \sum_{j=0}^{i-1} \mathcal{H}_2(t - j/\nu) - \Delta^2 \sum_{j=0}^{i-1} \mathcal{H}_1^2(t - j/\nu).$$

One can write the second moment as

$$B_2(t) = \frac{1}{2}\left[B_1^2(t) + \binom{\Delta}{2} M_1(t) - \Delta^2 M_2(t)\right], \tag{A.9}$$

with the iterative functions satisfying

$$M_1(t) = H(t - 1/\nu)M_1(t - 1/\nu) + \mathcal{H}_2(t), \tag{A.10}$$

and

$$M_2(t) = H(t - 1/\nu)M_2(t - 1/\nu) + \mathcal{H}_1^2(t) \tag{A.11}$$

After Laplace transforming equations (A.10) and (A.11) along similar lines to the first moment, we obtain the steady states

$$\lim_{t\to\infty} M_1(t) = \frac{\nu}{2\kappa}\rho_{\bar{k}}, \quad \lim_{t\to\infty} M_2(t) = \nu\widehat{\mathcal{H}_1^2}(0). \tag{A.12}$$

Performing the integration

$$\widehat{\mathcal{H}_1^2}(s) = \frac{2}{2\kappa + s}\int_0^\infty \int_y^\infty e^{-\kappa(y'-y) - sy'} dF(y', \bar{k}) dF(y, \bar{k}),$$

setting $s = 0$, and changing variables gives

$$\widehat{\mathcal{H}_1^2}(0) = \frac{\rho_{\bar{k}}^2}{\kappa}\mathcal{I}_{\bar{k}}(\kappa), \quad \mathcal{I}_{\bar{k}}(\kappa) = \int_0^\infty e^{-\kappa y'} \int_0^\infty f_{\bar{k}}(y) f_{\bar{k}}(y + y') dy dy'.$$

This then generates the steady-state second binomial moment

$$B_2^* = \frac{1}{2}\left[B_1^{*2} + \binom{\Delta}{2}\frac{\nu}{2\kappa}\rho_{\bar{k}} - \frac{\nu\Delta^2}{\kappa}\rho_{\bar{k}}^2\mathcal{I}_{\bar{k}}(\kappa)\right]. \tag{A.13}$$

Using the fact that

$$\langle N^2\rangle - \langle N\rangle^2 = 2B_2^* + B_1^* - B_1^{*2},$$

we thus obtain the steady-state variance (4.8).

Acknowledgements

PCB was supported by the National Science Foundation (DMS-1613048).

[1] Bateson P and Gluckman P 2012 Plasticity and robustness in development and evolution. *Int. J. Epidemiol.* **41** 219-223.
[2] Bressloff P C and Newby J M 2013 Stochastic models of intracellular transport. *Rev. Mod. Phys.* **85** 135-196.
[3] Bressloff P C 2014 *Stochastic Processes in Cell Biology* Springer Berlin
[4] Bressloff P C and Kim H (2018) Bidirectional transport model of morphogen gradient formation via cytonemes. *Phys. Biol.* **15** 026010.
[5] Bressloff P C and Kim H (2019) Search-and-capture model of cytoneme-mediated morphogen gradient formation *Phys. Rev. E* **99** 052401.
[6] Du L, Sohr A, Yan G, and Roy S (2018) Feedback regulation of cytoneme-mediated transport shapes a tissue- specific FGF morphogen gradient *eLife* 7:e38137.
[7] Gopalakrishnan M and Govindan B S 2011 A first-passage-time theory for search and capture of chromosomes by microtubules in mitosis. *Bull. Math. Biol.* **73** 2483-2506.
[8] Gradilla A C and Guerrero I 2013 Cytoneme-mediated cell-to-cell signaling during development. *Cell Tissue Res.* **352** 59-66.
[9] Huang H and Kornberg T B 2015 Myoblast cytonemes mediate Wg signaling from the wing imaginal disc and Delta-Notch signaling to the air sac primordium. *eLife* 4:e06114.
[10] Kim H and Bressloff P C 2018 Direct vs. synaptic contacts in a mathematical model of cytoneme-based morphogen gradient formation *SIAM J. Appl. Math* **78** 2323-2347.
[11] Kornberg T B 2014 Cytonemes and the dispersion of morphogens. *WIREs Dev Biol* **3** 445-463.
[12] Kornberg T B and Roy S 2014 Cytonemes as specialized signaling filopodia. *Development* **141** 729-736.
[13] Kumar N, Singh A and Kulkarni R V 2015 Transcriptional bursting in gene expression: analytical results for general stochastic models. *PLoS Comp. Biol.* **11** e1004292.
[14] Mulder B M 2012 Microtubules interacting with a boundary: Mean length and mean first-passage times. *Phys. Rev. E* **86** 011902.
[15] Norris J R 1998 Markov Chains. Cambridge Series in Statistical and Probabilistic Mathematics.
[16] Roy S, Hsiung F, and Kornberg T B 2011 Specificity of Drosophila cytonemes for distinct signaling pathways. *Science* **332** 354-358.
[17] Sanders T A, Llagostera E, and Barna M 2013 Specialized filopodia direct long-range transport of SHH during vertebrate tissue patterning. *Nature* **497** 628-632.
[18] Stanganello E et al. 2015 Filopodia-based Wnt transport during vertebrate tissue patterning *Nat. Comm.* **6** 5846.
[19] Stanganello E and Scholpp S 2016 Role of cytonemes in Wnt transport *J. Cell Sci.* **129** 665-672.
[20] Sohr A, Du L, Wang R, Lin L, and Roy S 2019 *Drosophila* FGF cleavage is required for efficient intracellular sorting and intercellular dispersal *J. Cell. Biol.* **218** 1653-1669
[21] Teimouri H and Kolomeisky A B 2015 A New Model for Understanding Mechanism of Biological Signaling: Direct Transport via Cytonemes *J. Phys. Chem. Lett.* **7** 180-185.
[22] Wolpert L 1969 Positional information and the spatial pattern of cellular differentiation *J. Theor. Biol.* **25** 1-47